Structure of thermal donors (NL8) in silicon: A study with electron-nuclear double resonance

J. Michel, J. R. Niklas, and J.-M. Spaeth
Faculty of Physics, University of Paderborn, Warburger Strasse 100A, D-4790 Paderborn, Federal Republic of Germany
(Received 14 November 1988; revised manuscript received 20 March 1989)

Singly ionized thermal donors [$(TD)^+$], which give rise to the NL8 ESR spectrum, were investigated with electron-nuclear double resonance (ENDOR) in B-doped Czochralski-grown silicon and float-zone silicon into which the magnetic isotope ^{17}O was diffused. TD's were formed by annealing at 460 °C for 2–8 h. ENDOR lines of two shells of ^{17}O and seven shells of ^{29}Si were observed. Five different species of TD^+'s were identified, which are formed one after another upon annealing. The ESR spectra of these TD's were superimposed in the NL8 spectrum. The smallest TD^+ measured by ENDOR is probably identical with TD_3^+ as identified from the infrared-absorption bands. The core of the TD's contains four oxygen atoms, two on each of the two (110) mirror planes. All the five TD^+'s investigated showed C_{2v} point-group symmetry. A single Si atom is possibly also part of the TD core structure, while the other Si neighbors are ligands. The hyperfine interactions of all ^{29}Si and ^{17}O nuclei are very small, representing only about 5% of the unpaired-electron spin density. The small size of the interactions cannot be explained by present theories. The compatibility of current TD models with the ENDOR results is discussed.

I. INTRODUCTION

Silicon crystals grown in quartz crucibles using the Czochralski (Cz) method contain a high concentration of interstitial oxygen ($10^{18}/cm^3$). Upon annealing at temperatures around 450 °C, electrically active "shallow" defects are formed, which have energy levels near the conduction band. Although the existence of these defects has been known for over 30 years,[1–3] there is no agreement yet with regard to either their atomistic structure or the number of distinct heat-treatment centers. Since Si-device processing requires several heat treatments, it is also of technological importance to understand these centers.

Upon annealing undoped Cz-Si at 450 °C, a shallow double donor is formed, which generally is called the "thermal donor (TD)."[3] We will henceforth restrict the name TD to this species of heat-treatment centers. Sometimes all heat-treatment centers are called thermal donors, although it is not clear whether they all are really donors.[4,5]

In early work, TD's were thought to consist of oxygen clusters. Kaiser *et al.*[3] found the initial growth rate to be proportional to the fourth power of the initial oxygen concentration. They speculated that TD's are SiO_4 complexes. More recently, the question has arisen as to whether the TD cores contain oxygen at all.[6,7] It was argued that oxygen could replace substitutional Si and create interstitial Si, which then clusters to form TD's.[6] A self-interstitial model based on formation kinetics has also been proposed recently.[7]

By investigating the infrared-(ir) absorption bands, Wagner *et al.*[8] and Pajot *et al.*[9] identified the TD's as a series of up to nine defect species, which were formed one after another upon annealing. From these investigations, the TD energy levels were shown to be effective-mass-like, differing by about 2 meV from species to species. Both TD's and $(TD)^+$'s possess a series of bands in their ir-absorption spectra. TD's can be singly ionized [$(TD)^+$] by doping with acceptors. $(TD)^+$'s are paramagnetic; therefore, ESR and electron-nuclear double resonance (ENDOR) can be applied in the study of their atomistic structure. Upon annealing *p*-type Cz-Si at 450 °C for short times (from 30 min to several hours), mainly the so-called "NL8" TD^+ defects appear, whereas upon longer times (on the order of 100 h), mainly the "NL10" defects are formed.[8–11] The ESR spectrum of the NL8 centers indicates defects having C_{2v} symmetry with *g* factors near 2 and no resolved hyperfine structure.

From ESR and ir investigations with uniaxial stress, the NL8 ESR spectrum was correlated with the singly ionized TD's.[12,13] It was concluded that the whole series of $(TD)^+$'s must have their ESR spectra superimposed on the NL8 ESR spectrum.[12,13] This was confirmed by ENDOR experiments of NL8 defects in which the ^{29}Si superhyperfine (shf) interactions could be resolved.[14] From this ENDOR study it could not be decided whether the TD core contains oxygen, since nearly 100% of the oxygen isotopes occurring naturally in the Cz-Si have no magnetic moment and therefore exhibit no shf interactions. Recently, in float-zone (FZ) Si, into which the magnetic isotope ^{17}O was diffused, ENDOR experiments resolved ^{17}O hyperfine interactions and proved that oxygen does indeed form part of the TD structure.[15,16] A similar recent experiment on NL10 defects in Al-doped Si showed that oxygen is also involved in this heat-treatment center.[17,5] NL10 defects are, however, different defects and are not related to NL8.[18]

It is the purpose of this paper to give a full account of

our ESR and ENDOR experiments and analysis with respect to the NL8 $(TD)^+$ defects in Cz-Si and ^{17}O-diffused FZ-Si. It will be shown that the core of the defect contains four oxygen atoms on the two (110) mirror planes of the defect, and that within experimental accuracy the C_{2v} symmetry of NL8 does not change during the subsequent formation of the TD upon annealing. Using ENDOR, we identified five $(TD)^+$ species. At each state of growth, the TD species become more shallow, as seen from the ir spectra.[8,9] ENDOR results correlate this movement of the defect level with an increased delocalization of the unpaired spin. However, from our present ENDOR experiments the reason for this delocalization is still unclear. If this delocalization is due to changes of the TD structure upon annealing, the change must occur outside the TD core. According to our ENDOR experiments, the atomistic structure of the core remains unchanged. It is commonly believed that additional oxygen atoms are attached to the TD's upon growth. Further ENDOR experiments with the aim of detecting distant oxygen atoms are currently being undertaken. Hopefully, these experiments will provide further information on the TD structure during growth.

II. EXPERIMENT

A. ESR and ENDOR measurements

ESR and ENDOR measurements were performed in an X-band custom-built computer-controlled ENDOR spectrometer using the stationary ENDOR method.[19] The sample temperature could be varied between 3.5 K and room temperature. The stationary ENDOR of NL8 centers could be measured best between 10 and 45 K depending on the resistivity of the sample. The stationary ENDOR of NL10 defects could be observed only at 8 K and below, not at higher temperature, due to its shorter spin-lattice relaxation time compared to NL8. Therefore NL8 ENDOR can be measured independently in the presence of NL10.

Approximately 10^{-5} W of microwave power was applied to a cylindrical TE_{011} cavity with a loaded Q of about 10 000.

The rf was chopped at a frequency of 1 kHz, and the change of the ESR absorption signal was detected using the usual lock-in technique.

Due to the low abundance of the ^{29}Si nuclei (4.7%) and the low NL8-center concentration of about 3×10^{15} cm^{-3}, the ENDOR signals were very weak. Multiple scanning and averaging was necessary. In contrast to usual stationary ENDOR, the magnetic field was also modulated with frequencies on the order of 100 kHz. This modulation resulted in a signal-to-noise improvement by about a factor of 10, in contrast to systems with a high abundance of magnetic neighbor nuclei, where such a modulation had a detrimental effect.[20] The modulation frequency was computer controlled such that the ratio between the ENDOR frequency and the modulation frequency was always constant. This was essential to avoid spurious signals.[20] In order to measure a complete angular dependence of the ENDOR lines for one plane of rotation, continuous measurements were needed for up to about 6 weeks. A characteristic feature of the ENDOR spectra was that many ENDOR lines appeared in a rather narrow frequency range and were therefore superimposed. In order to determine the line positions, the spectra were treated with digital filtering, automatic background subtraction, and special algorithms for peak searching and deconvolution.[20–22] The samples could be illuminated during the measurements with monochromatic and white-light trough slots in the microwave cavity.

B. Sample preparation

The samples were prepared from material provided by P. Wagner, W. Zulehner, and M. Stavola. Three Cz-grown Si samples were examined: sample 1 (Si-1) contained 4.5×10^{15} B/cm^3 and 10^{18} O/cm^3; sample 2 (Si-2) contained 1.2×10^{15} B/cm^3 and 9×10^{17} O/cm^3, and sample 3 (Si-3) contained 7×10^{15} B/cm^3 and 10^{18} O/cm^3 (Si-3).

All the samples were annealed at 770 °C for 15 min to ensure the same starting condition for the formation of TD's. Annealing at 460 °C was applied for 1.5, 2, 3, 4, 6, and 8 h to produce TD's. The annealing was done in a resistance-heated furnace under N_2-gas atmosphere with a few vol. % O_2 to avoid oxygen out-diffusion.

The magnetic oxygen isotope ^{17}O was diffused into FZ-Si doped with 5.7×10^{15} B/cm^3. In order to avoid contamination with transition metals such as Fe or Ti, the diffusion was done under extremely clean conditions using an ir heat chamber (type E4-2, Research, Inc.), the cross section of which is shown in Fig. 1. The sample rod (diameter 3 mm, length 75 mm) was mounted in the common focal line of four elliptical mirrors, while four halogen lamps are in the four other focal lines. The sample is placed into an O_2-gas atmosphere, enriched to 70% with ^{17}O, in a cooled quartz ampoule onto a short quartz rod (see Fig. 2). The sample was held for about 14 d at an oxygen pressure of 3 bars at 1400 °C. The temperature gradient was within 5% over 50 mm of the sample length. The hottest point in the ampoule and support system

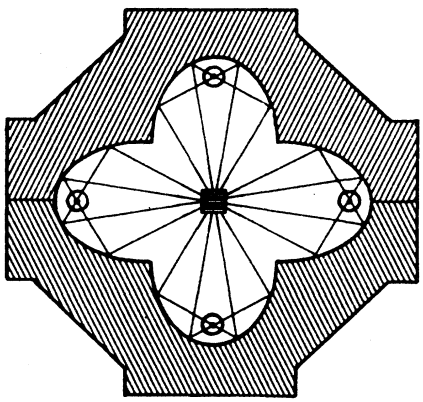

FIG. 1. Cross section of ir heat chamber.

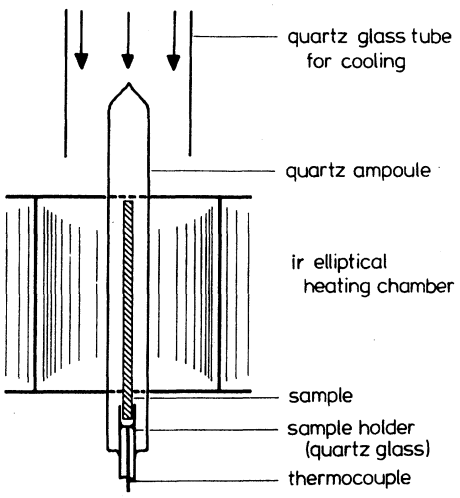

FIG. 2. Arrangement of quartz ampoule with silicon sample for diffusion of ^{17}O.

could be held below 900 °C by forced air cooling, thus over 500 °C less than the sample temperature. The quartz tube showed no changes in color or shape after 14 d. No traces of metal contamination were found in the ESR or ENDOR spectra. After the diffusion, the sample material contained a total interstitial oxygen concentration of 1.1×10^{18} cm^{-3}, of which 54.5% (6.0×10^{17} cm^{-3}) was ^{17}O as measured by ir absorption.[23] No unusual formation of TD's, compared with Cz-Si, was observed.

III. EXPERIMENTAL RESULTS

A. ESR spectra

The ESR of $(TD)^+$ defects was only seen in p-type Si, since only singly ionized TD's are paramagnetic. However, the number of TD's formed by heat treatment and the number of B acceptors in the sample must be chosen in an appropriate way. Figure 3 shows this schematically. If $2N_{TD} < N_B$, then all TD's are doubly ionized and no ESR is observable. If $N_{TD} = N_B$, then all formed TD's can be observed in ESR as $(TD)^+$. When $0.5N_B < N_{TD} < N_B$, then the ESR signal can be enhanced by illumination with light by ionizing B acceptors or by raising electrons from the valence band into $(TD)^+$ states. For $N_{TD} > N_B$, the number of ESR-observable $(TD)^+$'s is unchanged and diamagnetic TD's are formed. Figure 4(a) shows the ESR spectrum of $(TD)^+$ (NL8) defects in a Cz-Si sample (annealed 4 h at 460 °C) for $\mathbf{B}_0 \| [111]$, and Fig. 4(b) shows its angular dependence for rotation of the magnetic field in a (110) plane. The appearance of two lines in Fig. 4(a) is due to the six different center orientations, which are marked 1–6 in Fig. 4(b). For $\mathbf{B}_0 \| [111]$, the ESR spectra of three orientations coincide, giving two lines for the six orientations (see also Sec. IV B 2). No ligand hyperfine interactions (shf) or hyperfine (hf) interactions are resolved in the ESR spectrum. A careful search for weak hf satellite lines was undertaken. In the magnetic field range up to 6 mT above and below the lines of Fig. 4(a), no further lines were observed with a relative intensity of $\geq$ 1:2000 compared to the line intensities measured at 337.5 and 338.5 mT, respectively. Within an intensity ratio of 1:500, no further lines were found for a magnetic field range up to 40 mT. Also, the ^{17}O-diffused Si sample showed no resolved hf interaction after $(TD)^+$ formation. The ESR lines exhibit a half-width of 0.4 mT.

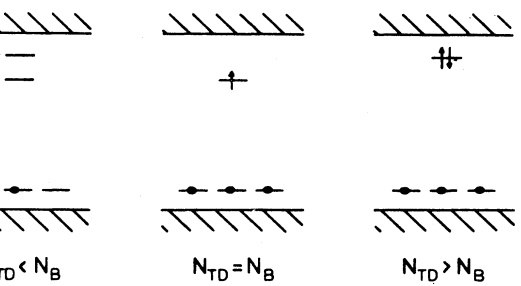

FIG. 3. Charge states of thermal donors as a function of the number of thermal donors. For details, see text.

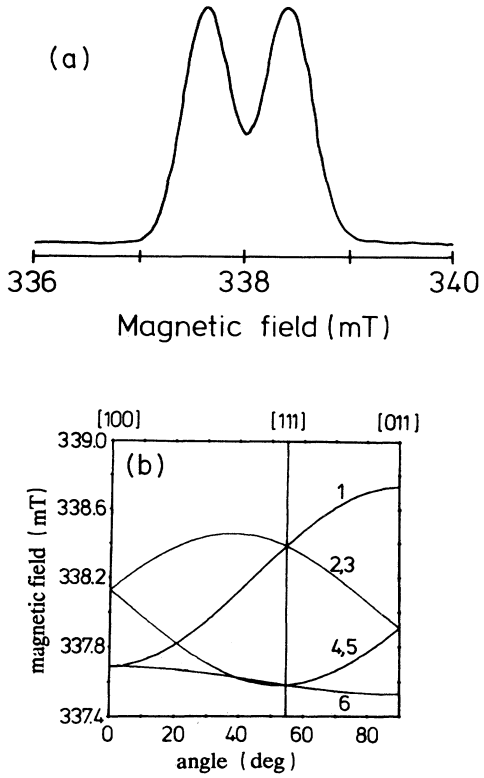

FIG. 4. (a) ESR absorption spectrum χ'' of $(TD)^+$ (NL8) for a Cz-Si sample annealed for 4 h at 460 °C. Magnetic field $\mathbf{B}_0$ parallel to [111], X band, $T = 30$ K. The ordinate is the ESR signal in arbitrary units. (b) Angular dependence of the $(TD)^+$ ESR spectrum for rotation of the magnetic field in a {110} plane. 1–6 denote the six center orientations. $(TD)^+$ has C_{2v} symmetry.

The ESR spectra were analyzed using the spin Hamiltonian,

$$\tilde{H}=g_e\mu_B\mathbf{B}_0\cdot\mathbf{S}\ , \tag{1}$$

with $S=\frac{1}{2}$, where the symbols have their usual meaning: g_e is the electron g value, μ_B is the Bohr magneton, $\mathbf{B}_0$ is the static magnetic field, and $\mathbf{S}$ is the electron-spin operator.

The spectrum has C_{2v} symmetry with the principal g values $g_1=1.99323$ (axis $\|[110]$), $g_2=2.00091$ (axis $\|[1\bar{1}0]$), and $g_3=1.999\,91$ (axis $\|[001]$). The symmetry of the defect is characterized by two (110) mirror planes perpendicular to each other which intersect in the [001] axis.[10]

B. ENDOR spectra

Figure 5(a) shows a typical $(TD)^+$ ENDOR spectrum measured in Cz-Si after 4 h of annealing (material Si-1). There is a strong line at the Larmor frequency ν_k of ^{29}Si due to many nuclei with a very weak shf interaction. The lines due to the ligand nuclei with stronger interactions between 4 and 8 MHz are much weaker. The sample contained about 3×10^{15} cm^{-3} $(TD)^+$'s. The weak signal had to be accumulated for a long period of time [10 h for the spectrum in Fig. 5(a)]. Omitting the strong line at ν_k yields the spectrum of Fig. 5(b). It shows many ENDOR lines up to about 8 MHz, many of which are not fully resolved due to superposition of the lines. The lines below 4.5 MHz are too numerous to be resolved in spite of the application of deconvolution procedures. By measuring the ENDOR spectra for different magnetic fields, which was achieved by changing the resonance frequency of the cavity and the microwave frequency accordingly, it was verified that all the ENDOR lines in Fig. 5(b) are due to ^{29}Si (also see below). Thus, no ENDOR lines of the two magnetic B isotopes ^{10}B ($I=3$, 20% abundance) and ^{11}B ($I=\frac{3}{2}$, 80% abundance) were detected. If the acceptor B was an integral part of the TD, one should observe ENDOR lines due to the two isotopes ^{10}B and ^{11}B. It has to be concluded that the acceptor does not influence the formation of NL8 TD's. ENDOR spectra of NL8 defects in Al-doped Cz-Si are identical to those measured in B-doped Cz-Si. No ^{27}Al ENDOR lines were detected, confirming that the NL8 $(TD)^+$ defect does not contain any acceptor dopant in the core of the structure.[18] Figure 6 shows the ^{29}Si ENDOR lines due to subsequent annealing at 460 °C for 2 h [Fig. 6(c)], 4 h [Fig. 6(b)], and 8 h [Fig. 6(a)] in Cz-Si. The $\mathbf{B}_0\|[111]$ orientation was used since the spectrum due to

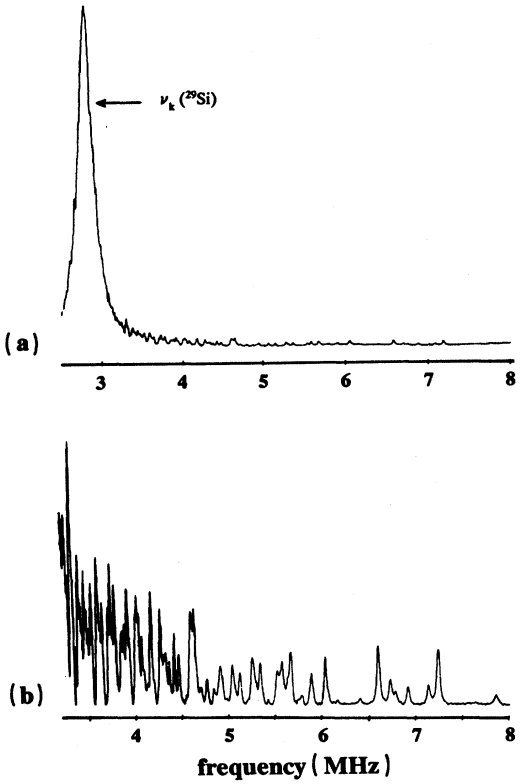

FIG. 5. (a) Section of the $(TD)^+$ ENDOR spectrum (ENDOR signal in arbitrary units) for Cz-Si after 4 h of annealing (material Si-1). $\mathbf{B}_0\|[111]$, $T=42$ K. The ordinate is the ENDOR signal in arbitrary units. (b) Upper frequency part of the spectrum of (a) with the strong line at ν_k(^{29}Si) omitted.

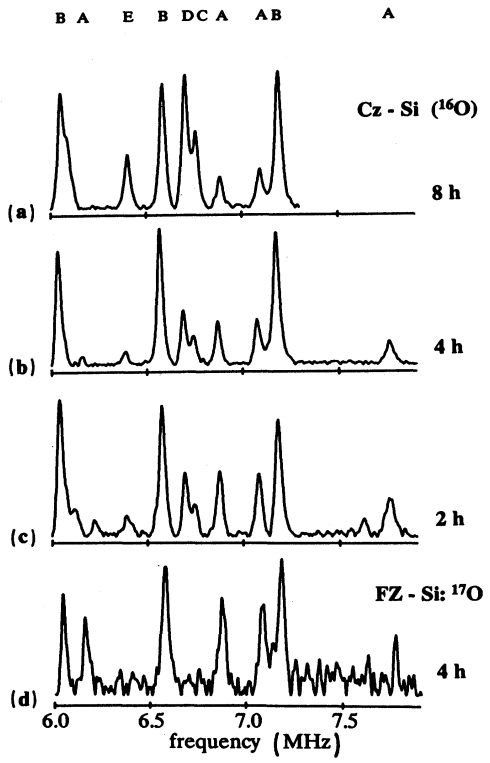

FIG. 6. Influence of annealing at 460 °C on the $(TD)^+$ (NL8) ^{29}Si ENDOR lines. $A-E$ denote the $(TD)^+$ species (see text). The ordinate is the ENDOR signal in arbitrary units. (a) 8 h annealing time, (b) 4 h annealing time, (c) 2 h annealing time, and (d) FZ-Si, into which ^{17}O has diffused, after 4 h annealing time.

coincidence of lines is particularly simple. The same ENDOR frequencies are observed in all three samples. There is, unfortunately, no reliable information on the center concentration from the ENDOR line intensities. However, relative intensities of lines in a spectrum reasonably reflect the relative concentrations of different defect species corresponding to these lines. Inspection of Figs. 6(a)–6(c) shows that the relative ENDOR line intensities do vary upon annealing time. As an example, the two lines at 7.07 and 7.14 MHz change their relative intensities quite markedly, with the line at 7.07 MHz decreasing upon increasing annealing time. The same relative change of the line intensities is found for several ENDOR lines in the frequency range between 6 and 8 MHz. These findings show that several $(TD)^+$ species are present simultaneously in the ENDOR spectrum and that their relative concentration changes within increasing annealing time. This behavior is in agreement with the results obtained from the ir measurements on $(TD)^+$.[9] In Fig. 6 the five different species thus identified are labeled $A-E$, with A being the species which appears first with increasing annealing time. In the short annealing time of 2 h, already five species were found. The weak ENDOR line at 7.6 MHz in Fig. 6(c) is probably associated with an "earlier" $(TD)^+$ species. Other $(TD)^+$'s with ENDOR lines below 6 MHz could not be identified because of the many superimposed lines in this frequency range.

An unsuccessful attempt was made to distinguish superimposed ESR spectra of the different $(TD)^+$ species by measuring ENDOR-induced ESR, which is a type of excitation spectroscopy of the ENDOR lines.[24] The differences in g factors or ESR linewidth for the different species were too small to be detected.

Figure 6(d) shows the ENDOR spectrum of ^{17}O-diffused FZ-Si after 4 h of annealing in the same frequency range, again for the $\mathbf{B}_0 \| [111]$ orientation. From comparison with Fig. 6(c), the same ENDOR lines appear that were assigned to $(TD)^+$ species A and B. Thus, by forming $(TD)^+$ defects in the oxygen-diffused FZ-Si, identical $(TD)^+$ defects are formed. The ENDOR lines of Fig. 6(c), i.e., after short annealing time (material Si-1), could only be measured under illumination with band-gap light, since the concentration of $(TD)^+$ formed by short annealing was smaller than half of the B concentration (see Sec. II), and all formed TD's are doubly ionized. With band-gap light of suitable intensity, ENDOR signals can be observed. If the light intensity is too high, diamagnetic TD's are created which diminish the ENDOR signals. Different $(TD)^+$ species can be distinguished by varying the light intensity.

Figure 7(b) shows the effect of illumination with 1.17-eV light for Si-1 after 4 h of annealing at 460 °C. Species A decreases while species B increases, as indicated schematically in Fig. 7(a). By changing relative ENDOR line intensities by illumination and varying annealing times, we observed results that were identical to the assignment of the ENDOR lines to specific species based on annealing studies.

A direct energy-level population of specific $(TD)^+$ species in samples with short annealing time (<2 h) by light was not possible. The energy levels differ by 6 meV,[8] which would require light of a photon-energy–distribution half-width below 2 meV intense enough to populate enough $(TD)^+$'s to measure ENDOR. Our light source and monochromator did not provide light with the required narrow bandwidth with enough intensity. A tunable laser emitting at about 1 eV photon energy would be required for such experiments.

In order to correlate the ENDOR experiments with the $(TD)^+$ ir bands, ir-absorption measurements were carried out on the samples measured in ENDOR. A precise 1:1 correlation between the ENDOR species $A-E$ and the $(TD)_1^+-(TD)_7^+$ ir species in our samples was not possible because of experimental difficulties. The ENDOR line intensities do not reflect precisely the corresponding concentrations because of their dependence on the spin-lattice relaxation time and cross-relaxation time,[19] which varied for the different annealing times. This was seen from the different temperatures in the range between 10 and 45 K for which the ENDOR effect was optimal. The ir-absorption cross section does also vary by about a factor of 5.[23] However, the general trends observed in ir were also found in ENDOR: those ENDOR lines at high frequencies—that is, for ^{29}Si nuclei

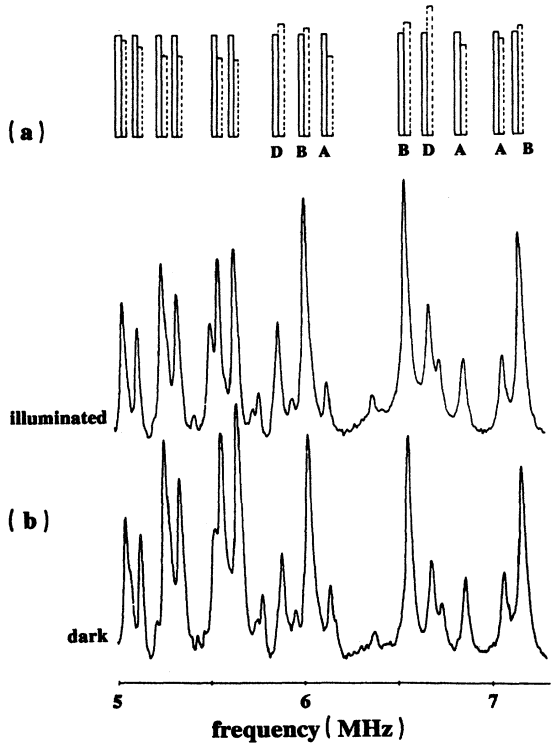

FIG. 7. Effect of illumination with 1.17-eV light on ^{29}Si ENDOR line intensities. The ordinate is the ENDOR signal in arbitrary units. (a) Schematic representation of intensity changes for the $(TD)^+$ species A, B, and D. The dotted lines correspond to the ENDOR line intensities with the sample illuminated. (b) ENDOR spectra of material Si-1 (4 h annealing at 460 °C) with and without illumination.

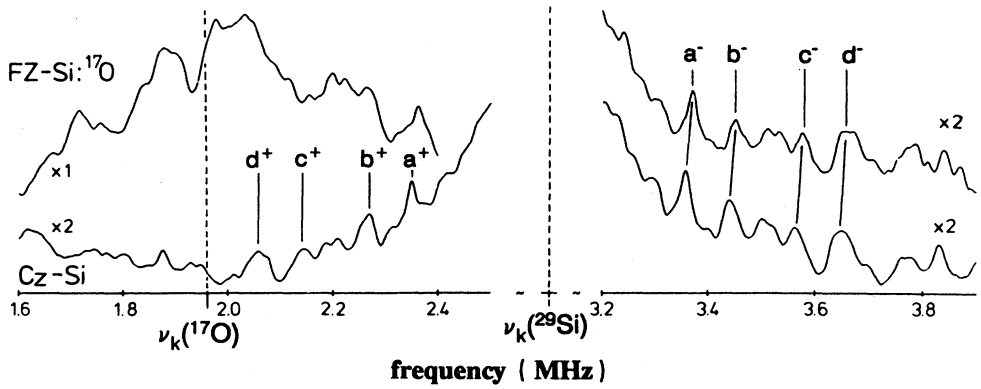

FIG. 8. $(TD)^+$ ENDOR spectra in FZ-Si with diffused ^{17}O (upper trace) and in Cz-Si (lower trace). The lines belong to defects A^+ and B^+. a–d refer to ^{29}Si ENDOR lines for $m_s=\pm\frac{1}{2}$. The ordinate is the ENDOR signal in arbitrary units.

with high interactions, which means a relatively high electron localization—do anneal out first and the new ENDOR lines of later species have smaller interactions. This correlates with the ir observations that the earlier species have deeper energy levels compared to the later ones. The more shallow a state, the more delocalized the electron distribution. From the comparison of the ENDOR results with the ir measurements, we conclude tentatively that the ENDOR species A is identical to the ir species $(TD)_3^+$, and that we have failed to see the two first species, which die out at a relatively early annealing stage,[8] in which their total concentration was not large enough to be observed by ENDOR.

Figure 8 shows the ENDOR spectrum of $(TD)^+$ defects measured in the ^{17}O-diffused FZ-Si for the low-frequency range (upper trace) in comparison to a sample containing $(TD)^+$ defects in Cz-Si ($[B]=4.5\times10^{15}$ cm^{-3}) after 3 h annealing (lower trace). Both samples contained only $(TD)^+$ species A and B, which was observed in the ENDOR spectrum between 6 and 8 MHz.

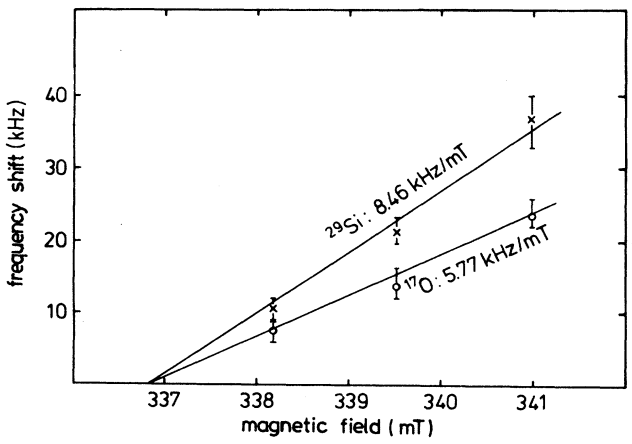

FIG. 9. ENDOR line positions for ^{29}Si and ^{17}O isotopes as a function of magnetic field.

The spectra of the two samples differ markedly between 1.6 and 2.5 MHz—that is, around the Larmor frequency of ^{17}O—while they are identical in the frequency range from 3.2 to 3.9 MHz. The lines a^+, b^+, c^+, and d^+, and a^-, b^-, c^-, and d^-, are due to ^{29}Si and are placed symmetrically about the Larmor frequency of ^{29}Si, as expected for weak shf interactions [see Eq. (5)]. The + and − signs refer to $m_s=\pm\frac{1}{2}$.[19]

The lines around $\nu_k(^{17}O)$ in the FZ-Si are due to ^{17}O nuclei. This was confirmed by measuring the shift of their frequency position as a function of the magnetic field (Fig. 9). This was realized by changing the resonator frequency and the microwave frequency accordingly. The ENDOR line position as function of magnetic field is expected to be dependent on the nuclear moment and nuclear g factor g_I of the nucleus, respectively (see next section). The straight lines in Fig. 9 are calculated according to Eq. (5) for the ^{29}Si and ^{17}O isotopes. Indeed, ENDOR lines of ^{17}O were measured and thus oxygen does form part of the $(TD)^+$ structure.

IV. ANALYSIS OF ENDOR SPECTRA

A. Superhyperfine interactions

The frequency of each ENDOR line in Fig. 5 is determined by the interaction energy of the electron spin of one NL8 species with the nuclear spin of one particular neighbor nucleus of this species. These shf interactions are introduced in the following spin Hamiltonian:

$$\tilde{H}=g_e\mu_B\mathbf{B}_0\cdot\mathbf{S}+\sum_i(\mathbf{I}_i\cdot\overleftrightarrow{\mathbf{A}}_i\cdot\mathbf{S}+\mathbf{I}_i\cdot\overleftrightarrow{\mathbf{Q}}_i\mathbf{I}_i-g_{I_i}\mu_N\mathbf{B}_0\cdot\mathbf{I}_i)\ . \quad (2)$$

The sum runs over all neighbor nuclei with which an interaction occurs, and the symbols have their usual meaning. The quadrupole term, $\mathbf{I}\cdot\overleftrightarrow{\mathbf{Q}}\cdot\mathbf{I}$, does not contribute for neighboring silicon since $I(^{29}Si)=\frac{1}{2}$. It does contribute for nuclei with nuclear spin $I>\frac{1}{2}$; for example, ^{17}O with $I=\frac{5}{2}$. In order to determine the interaction constants and possible lattice positions of the neighbor nuclei, the interaction parameters of the spin Hamiltonian have to

be determined such that the calculated eigenvalues of the Hamiltonian coincide with the corresponding experimental data. For these calculations it is convenient to make some approximations. Since the shf and quadrupole interactions are small compared to the electron Zeeman interaction, there are no noticeable couplings between different neighbor nuclei.[19,25] They can therefore be treated independently. This leads to the Hamiltonian for one nucleus:

$$\tilde{H}_i = g_e \mu_B \mathbf{B}_0 \cdot \mathbf{S} + \mathbf{I}_i \cdot \overleftrightarrow{A}_i \cdot \mathbf{S} + \mathbf{I}_i \cdot \overleftrightarrow{Q}_i \cdot \mathbf{I}_i - g_{I_i} \mu_N \mathbf{B}_0 \cdot \mathbf{I}_i \ . \quad (3)$$

Due to the small shf interactions, the electron-spin operator $\mathbf{S}$ can be replaced by its expectation value $\langle \mathbf{S} \rangle$ in the hyperfine-interaction term. It is then sufficient just to diagonalize the following nuclear spin Hamiltonian for the calculations:

$$\tilde{H}_i^N = \mathbf{I}_i \cdot \overleftrightarrow{A}_i \cdot \langle \mathbf{S} \rangle + \mathbf{I}_i \cdot \overleftrightarrow{Q}_i \cdot \mathbf{I}_i - g_{I_i} \mu_N \mathbf{B}_0 \cdot \mathbf{I}_i \ . \quad (4)$$

A simple first-order solution of this Hamiltonian for the ENDOR frequencies ν yields

$$\nu = \frac{1}{h} | m_s W_{\text{shf}} - g_I \mu_N B_0 + W_q | \ , \quad (5)$$

where W_{shf} is the energy of the shf interaction and W_q is the quadrupole-interaction energy. Both energies do not depend on the magnetic field in first order. Equation (5) predicts that the frequency of an ENDOR line will have a linear dependence with respect to the magnetic field. Therefore, an experimental determination of the nuclear g value g_I of the nucleus giving rise to this ENDOR line is possible. This was discussed above (also see Fig. 9).

For a complete analysis of the ENDOR spectra, the first-order solution of Eq. (5) is, however, not accurate enough and a full diagonalization of the nuclear-spin Hamiltonian of Eq. (4) is necessary.

It is convenient to express the principal values A_{xx}, A_{yy}, and A_{zz} of the shf tensor $\overleftrightarrow{A}$ by the isotropic shf constant a and the anisotropic shf constants b and b':

$$\begin{aligned} a &= (A_{xx} + A_{yy} + A_{zz})/3 \ , \\ b &= (A_{zz} - a)/2 \ , \\ b' &= (A_{xx} - A_{yy})/2 \ ; \end{aligned} \quad (6)$$

b' describes a deviation from axial symmetry of the tensor.

Correspondingly the principal values Q_{xx}, Q_{yy}, and Q_{zz} of the quadrupole tensor $\overleftrightarrow{Q}$ are expressed by

$$q = Q_{zz}/2, \quad q' = (Q_{xx} - Q_{yy})/2 \ . \quad (7)$$

The orientations of the principal axes of the tensors can only be derived from the variation of ENDOR line frequencies upon rotation of the crystal with respect to the magnetic field.

B. Symmetries of neighbor shells and ENDOR line angular dependencies

1. Definition of neighbor shells

For the analysis of the many ENDOR lines it is suitable to distinguish between different groups of neighbor nuclei by the definition of different neighbor shells in the following way.

One arbitrarily chosen point on the [001] axis of the defect is defined as the "center" of the NL8. Each neighbor nucleus N_i is considered the origin of a corresponding vector V_i pointing from the neighbor N_i towards this center. One now considers the group of symmetry transformations which leaves the NL8 with C_{2v} symmetry unchanged. Let the elements of this group be characterized by 3×3 orthogonal matrices S_l. Application of all the elements S_l to one given neighbor vector V_i, e.g., $i=1$, will transform this vector into different other vectors. The set of neighbor nuclei corresponding to these vectors is termed "neighbor shell." It follows that all nuclei of a shell are of the same chemical identity and have the same distance from the center. To find another neighbor shell, one just has to take a different V_i (not a member of the first shell) and once again has to apply all the S_l to this neighbor, and so on. It follows that there are many neighbor shells, but only a few different types of shells. The following types are of importance for the analysis of the ENDOR data for the NL8 considering a defect orientation with $g_3 \| [001]$ (see Sec. III A).

Type-1 shell: The neighbor shell consists just of one nucleus. The principal axis system of its shf tensor is parallel to that of the electron g tensor. The neighbor is on the [001] axis. Its location on this axis, however, is not fixed by symmetry constraints. Only one neighbor shell with this symmetry containing one Si nucleus only can be identified unambiguously for each NL8 species.

Type-2 shell: The location of the neighbor nuclei is somewhere between the two $\{110\}$ mirror planes present because of the C_{2v} symmetry. Because of the two mirror planes, this shell contains four neighbors. All principal axes of the shf tensors for this shell were found to be

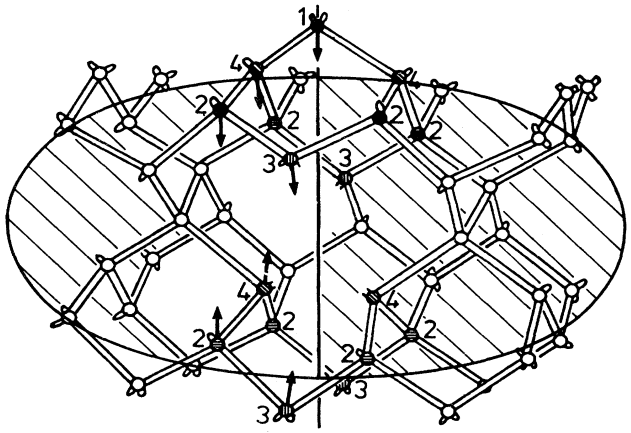

FIG. 10. Possible positions of Si neighbor nuclei in the lattice corresponding to different neighbor-shell symmetries denoted 1–4. The principal axes (z) of the shf tensors (with largest interaction) are indicated by arrows. The electron distribution according to the [001] two-valley combination is roughly indicated also (see text).

parallel to ⟨100⟩ directions of the crystal. This suggests that the corresponding neighbors are on {100} planes.

Type-3 shell: All neighbors of this shell are in one (110) mirror plane. There are two of those neighbors. The z axes (axes of largest shf interactions) of their principal-axis systems and the x axes are in this plane. The angle ϑ between the defect [001] axis and the tensor z axes is not determined by symmetry.

Type-4 shell: This shell has the same symmetry properties as the type-3 shell. However, the two neighbors are located in the (110) mirror plane perpendicular to that of the type-3 shell.

The positions of neighbor nuclei in the silicon lattice corresponding to these types of neighbor shells are shown in Fig. 10. There is no information from symmetry arguments about the distance of a neighbor shell to the "center" of the NL8. In Fig. 10 it is assumed that the different neighbor shells are as close to this center as their symmetry properties allow. The numbers at the neighbor sites denote the type of neighbor shell. Shells of type 2, 3, and 4 are present in the upper and lower part in the lattice.

2. *Symmetry properties of the electron g tensor and the shf and quadrupole tensors*

The shf interaction of a neighbor nucleus N_i, V_i with the unpaired electron spin of the NL8 is described by the term $\mathbf{I}\cdot\overleftrightarrow{\mathbf{A}}\cdot\langle\mathbf{S}\rangle$ in the nuclear-spin Hamiltonian of Eq. (4). Let the neighbor N_k, V_k be in the same neighbor shell as N_i, V_i ($i \neq k$). Then there exists a matrix S_l which transforms V_i into V_k, $V_k = S_l \times V_i$. The shf tensor for the neighbor N_i, V_i, $\overleftrightarrow{\mathbf{A}}_i$, is then simply transformed into that of the neighbor N_k, V_k, $\overleftrightarrow{\mathbf{A}}_k$, by $\overleftrightarrow{\mathbf{A}}_k = \mathbf{S}_l \times \overleftrightarrow{\mathbf{A}}_i \times \mathbf{S}_l'$. The same relations are valid for the quadrupole tensors. It follows that the shf constants a, b, b', the quadrupole constants q, q', and the angles ϑ (see type-3 shell) are the same for all members of a neighbor shell.

So far, it has not yet been taken into account that the symmetry of the NL8 is considerably lower than that of the silicon lattice. As a consequence, the NL8 exists in six different orientations in the lattice, which may be characterized by six orthogonal 3×3 matrices O_j, $j = 1, 2, \ldots, 6$. In a similar way as for the different members of a neighbor shell, all ENDOR frequencies calculated for one center orientation can be obtained for a different center orientation by transforming all tensors using a suitable matrix O_j. Figure 4(b) shows the ESR angular dependence pattern due to the electron g-value anisotropy when rotating the magnetic field in a {110} plane. The different lines are due to the different orientations of the NL8 centers in the lattice, which are denoted 1–6. The ESR lines for orientations 2 and 3 and for 4 and 5 are identical for rotating the magnetic field in a {110} plane. For the ENDOR measurements it is possible to measure ENDOR lines separately for different orientations, or at least for a selected couple of orientations by adjusting the magnetic field to the different lines in Fig. 4(b) during the experiments. This possibility facil-

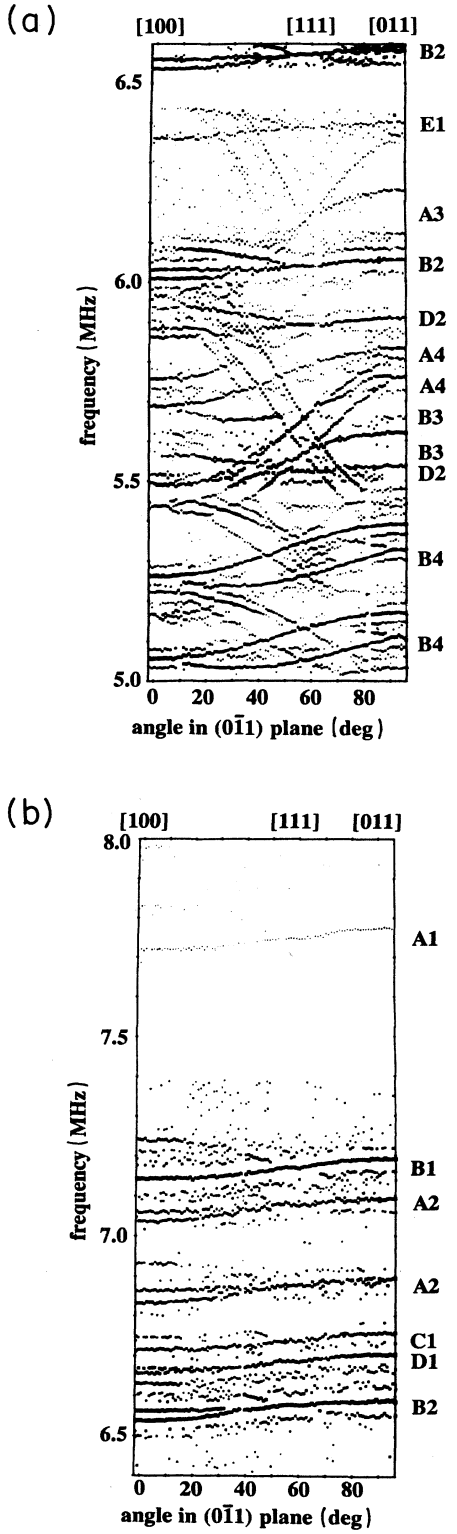

FIG. 11. Experimental ^{29}Si ENDOR angular dependence for rotation of the magnetic field $\mathbf{B}_0$ in a {110} plane. $\mathbf{B}_0$ was set to follow the ESR angular dependence of center orientations 4 and 5 [see Fig. 4(b)]. A–E denote the different $(TD)^+$ species, 1–4 the neighbor shells. The dots represent the line positions and the diameter of the dots is a rough measure of the line intensities: (a) lower-frequency range and (b) higher-frequency range.

itates the assignment of ENDOR lines to the different types of neighbor-shell symmetries.

3. *ENDOR angular dependencies*

ENDOR angular dependence results are shown in Fig. 11. The magnetic field was varied in the (110) plane starting along [100] (0°) and ending along [011] (90°). The field was adjusted for the different angles to the values corresponding to the center orientations 4 and 5 [see Fig. 4(b)]. $A-D$ denote the different NL8 species; 1–4 correspond to the neighbor-shell types explained above. All the data shown correspond exclusively to the interaction with ^{29}Si neighbor nuclei. The dots indicating the frequency variation of ENDOR lines upon rotation of the crystal do not appear as accurate as one might expect for high-precision ENDOR experiments. One has, however, to bare in mind that the concentration of the NL8 centers was of the order of $2\times10^{15}/\text{cm}^3$ and that the only magnetic silicon isotope, ^{29}Si, has a natural abundance of only 4.7%. Therefore the signal-to-noise ratio was a severe problem, and the collection of the data shown in Fig. 11 needed over 300 h of continuous measurement time. The dots exhibiting no systematic behavior in Fig. 11 correspond to stochastic noise in the ENDOR spectra. They were taken as line positions by the automatic peak-search algorithm. These dots, however, verify that no weak ENDOR lines have been overlooked within the many noise peaks.

ENDOR angular dependencies of ^{29}Si neighbors for the $(TD)^+$ B for different neighbor-shell symmetries and center orientations are shown in more detail in the following figures. The magnetic field was varied in the same way as described already for Fig. 11.

Data for the type-1 neighbor shell are illustrated in Fig. 12(a). The solid lines are calculated angular dependencies after determining the interaction parameters for the center orientations 4–6, according to the spin Hamiltonian of Eq. (4). Calculated angular dependencies for the remaining orientations 1–3 are shown in Fig. 12(b) for the same neighbor shell, together with those of orientations 4–6. Correspondingly, Figs. 13(a) and 13(b) show data for the type-2 shell, Figs. 14(a) and 14(b) for the type-3 shell, and Figs. 15(a) and 15(b) for the type-4 shell. The shf interaction constants are collected in Table I.

So far, only shf interactions for ^{29}Si nuclei were considered. Results for ^{17}O nuclei are shown in Fig. 16. The magnetic field was again varied in the same way as shown in Fig. 11. Only the nearly-angle-independent dots are due to ^{29}Si shf interactions. Because of the nuclear spin $I=\frac{5}{2}$ of ^{17}O, one expects 10 lines (five lines for each m_s state) for each neighbor nucleus, which makes the assignment of the experimental data to the different neighbor-shell symmetries and center orientations very difficult. However, the symmetry properties of the ^{17}O nuclei corresponding to the dots on the solid lines in Fig. 16(a) could be clearly identified. The solid lines are calculated with Eq. (4) after determining the shf and quadrupole parameters (Table I). The data correspond to two NL8 species denoted A and B with only very slightly different shf constants (note the "parallel" angular dependencies). Two different ^{17}O neighbor shells could be analyzed and

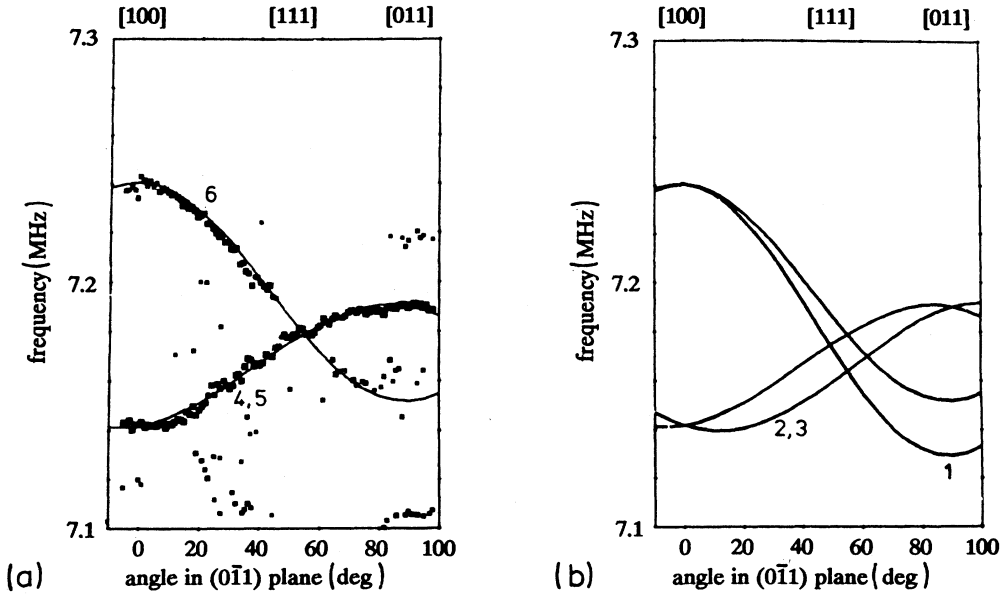

FIG. 12. ENDOR angular dependence for the $(TD)^+$ B for the type-1 neighbor shell. The numbers denote the center orientations. (a) Experimental data (dots) and calculated values (solid lines) after fitting of free parameters in the spin Hamiltonian [Eq. (4)] for the center orientations 4–6. (b) Calculated angular dependencies for all six center orientations [orientations 1–3 are marked; orientations 4–5 are as in (a)].

TABLE I. shf interaction constants of ^{29}Si neighbor shells for five different TD's. a, b, b', q, and q' in MHz; ϑ in degrees. For the neighbor shells marked with an asterisk, the assignment to their type of symmetry is not quite clear. shf and quadrupole constants are given for two oxygen shells for the two TD's A and B. Experimental uncertainty for the interaction constants is ±10 kHz; for the angle ϑ it is ±1°.

^{29}Si interactions

Shell type	(TD)$^+$ A a	b	b'	ϑ	(TD)$^+$ B a	b	b'	ϑ	(TD)$^+$ C a	b	b'	ϑ	(TD)$^+$ D a	b	b'	ϑ
1	9.89	0.07	0.03	0	8.72	0.07	0.02	0	7.86	0.06	0.02	0	7.75	0.06	0.02	0
2*a*	8.53	0.06	0.03	0	7.52	0.05	0.03	0	6.51	0.05	0.02	0	6.15	0.06	0.02	0
2*b*	8.12	0.06	0.03	0	6.45	0.04	0.03	0	5.20	0.04	0.02	0	5.42	0.04	0.02	0
3*a*	6.74	0.45	0.10	3.5	5.73	0.39	0.08	3.3	5.01	0.33	0.10	8.8	3.66*	0.24	0.06	13.8
3*b*	6.36	0.49	0.19	9.2	5.57	0.35	0.08	11.6	4.97	0.29	0.01	11.3				
4*a*	6.03	0.17	0.09	11.5	5.02	0.14	0.07	10.8	4.05	0.11	0.07	10.2	3.08*	0.08	0.05	10.3
4*b*	5.87	0.15	0.08	12.5	4.59	0.12	0.07	11.7	3.89	0.09	0.06	11.0				
1					3.31*	0.03	0.01	0								
1					3.21*	0.03	0.01	0								

Shell type	(TD)$^+$ E a	b	b'	ϑ
1	7.15	0.06	−0.02	0

^{17}O interactions

Shell type	(TD)$^+$ A a	b	b'	ϑ	q	q'	(TD)$^+$ B a	b	b'	ϑ	q	q'
1	−0.52	0.08	−0.07	58	0.11	0.09	−0.47	0.09	−0.08	58	0.11	0.09
2	−0.18	0.08	−0.07	62	0.12	0.05	−0.11	0.08	−0.06	62	0.11	0.04

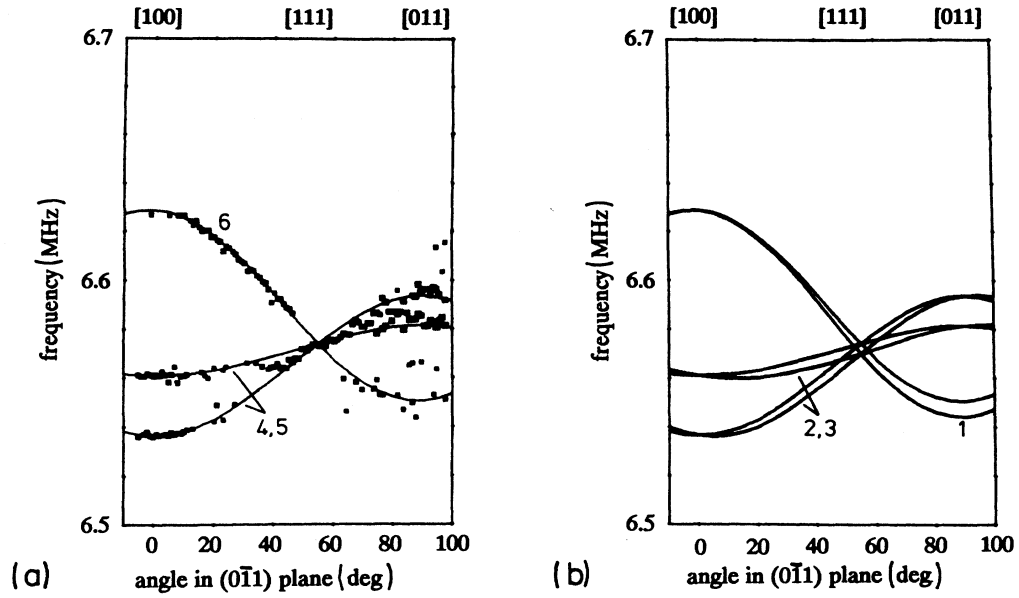

FIG. 13. ENDOR angular dependence for the $(TD)^+$ B for the type-2 neighbor shell. The numbers denote the center orientations. (a) Experimental data (dots) and calculated values (solid lines) after fitting of free parameters in the spin Hamiltonian [Eq. (4)] for the center orientations 4–6. (b) Calculated angular dependencies for all six center orientations [orientations 1–3 are marked; orientations 4–6 are as in Fig. 12(a)].

are denoted 1 and 2. The z axes of the shf and quadrupole tensors for these shells are in $\{110\}$ planes of the crystal. They all point nearly in $\langle 111 \rangle$ directions. This excludes the possibility of a single oxygen atom on the [001] axis of the NL8 (compare type-1 neighbor-shell symmetry). For clarity, not all the calculated angular dependencies are shown in Fig. 16(a). Figure 16(b) shows the angular dependence of ^{17}O shell 1 and Fig. 16(c) that

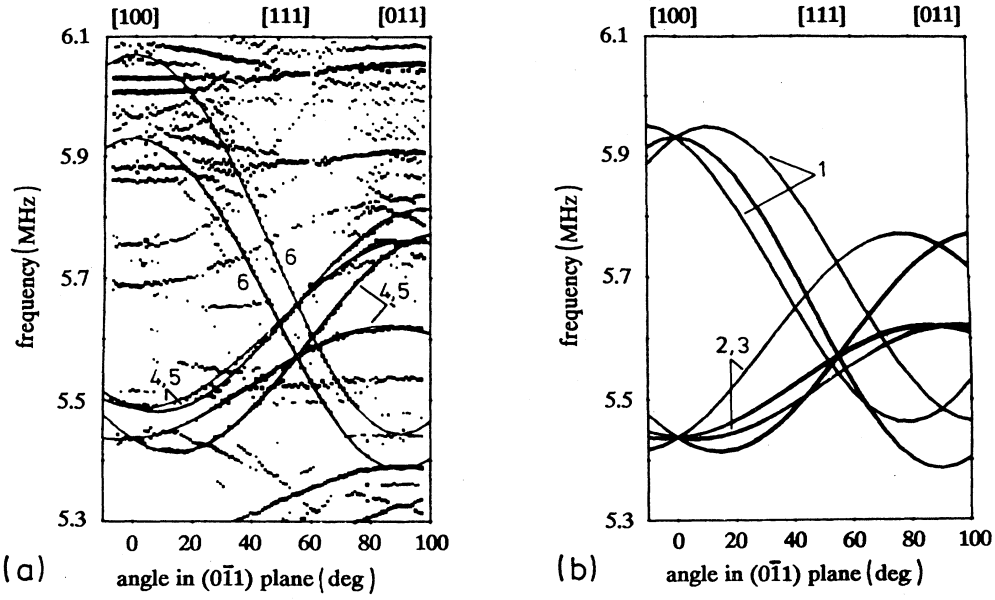

FIG. 14. ENDOR angular dependence for the $(TD)^+$ B for the type-3 neighbor shell. The numbers denote the center orientations. (a) Experimental data (dots) and calculated values (solid lines) after fitting of free parameters in the spin Hamiltonian [Eq. (4)] for the center orientations 4–6 for both type-3 neighbor shells. (b) Calculated angular dependencies for all six center orientations [orientations 1–3 are marked; orientations 4–6 are as in Fig. 12(a)].

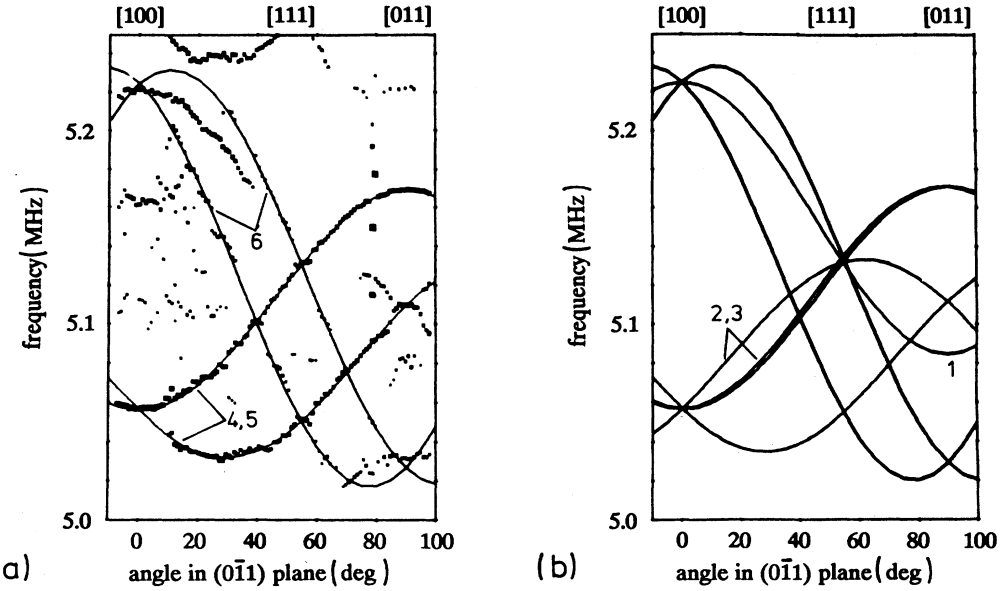

FIG. 15. ENDOR angular dependence for the $(TD)^+$ B for the type-4 neighbor shell. The numbers denote the center orientations. (a) Experimental data (dots) and calculated values (solid lines) after fitting of free parameters in the spin Hamiltonian [Eq. (4)] for the center orientations 4–6. (b) Calculated angular dependencies for all six center orientations [orientations 1–3 are marked; orientations 4–6 are as in Fig. 12(a)].

of ^{17}O shell 2. These calculated angular dependencies correspond to center orientation 2. The + and − signs correspond to the $m_s = +\frac{1}{2}$ and $-\frac{1}{2}$ values, respectively.

Due to the very many lines shown in Fig. 16, it was not possible to assign the analyzed oxygen neighbor nuclei definitely to particular "shell" symmetries as was done for the ^{29}Si nuclei. An interesting question is whether the C_{2v} symmetry with its characteristic two mirror planes is also conserved for the oxygen nuclei. If this was not the case, then these oxygen nuclei must be well separated in space from all analyzed Si nuclei, since for Si the C_{2v} symmetry was always obtained within the precision of an ENDOR line half-width (approximately 50 KHz). The assumption of such a large separation, however, seems very unlikely with respect to the Si and oxygen shf interactions. This argument leads one to conclude that the two mirror planes perpendicular to each other do also exist for the oxygen. Since each of the oxygen shf tensor z axes was analyzed to reside in a $\{110\}$ mirror plane, each oxygen must have an equivalent partner in the same shell due to the perpendicular mirror plane. Therefore we observed two neighbor shells of oxygen neighbors with two nuclei each, where each of the oxygen nuclei is in a $\{110\}$ plane with its tensor z axis approximately parallel to a $\langle 111 \rangle$ direction. This conclusion is supported by additional arguments. If there were only two oxygen atoms inside the core of the $(TD)^+$, then the ^{29}Si shell-2 nuclei would have four different shf interactions of comparable size taking only the nearest shell-2 nuclei (that are those above the core) into account (see Fig. 17). According to the geometrical situation, perhaps nuclei 2b and 2c (Fig. 17) have the same or nearly the same interactions. Then three different shell-2 interactions should have been observed. There are, however, only two different shell-2 interactions observed with their characteristic angular dependence of Fig. 13 (shells 2a and b in Table I).[16] This is only possible with the C_{2v} symmetry with four oxygen atoms in the core.

C. Results for shf- and quadrupole-interaction constants

Table I summarizes results for the isotropic shf constants a, the anisotropic constants b and b', and the quadrupole constants q and q' for the different neighbor shells. The data are obtained by fitting the parameters a,b,b',q,q' and the angle ϑ as free parameters in the spin Hamiltonian of Eq. (4) until calculated values of the Hamiltonian coincide with the experimental data for the different neighbor shells and center orientations.

V. DISCUSSION

A. Microscopic models of thermal donors

From our ENDOR results for ^{29}Si and ^{17}O nuclei, it is clear that upon TD growth no structural changes of the TD are likely to occur within that part of the structure, which contains the ENDOR-identified ^{29}Si and ^{17}O nuclei. All that happens from species to species is a decrease in shf constants (see Table I). Since the isotropic shf constant a is proportional to the unpaired spin density at the nuclear site,[25] this means that upon TD growth only the delocalization of the unpaired electron increases. It is in accordance with ir results that the energy levels become more and more shallow. The statement—that

the symmetry of all the five identified $(TD)^+$'s is C_{2v}—can only be made, of course, with the precision of the ENDOR linewidths. From our measurements, we cannot yet say whether upon growth further oxygen or, for example, interstitial Si is added to the defect. We have observed the largest ^{17}O shf interaction and therefore assigned those oxygen atoms to the core of the TD structure. If upon growth further oxygen atoms are added, then their shf interactions are expected to be smaller compared to those in the core and they will only contribute ENDOR signals near $\nu_k(^{17}O)$, which are not resolvable any more. Whether or not more and more "distant" ENDOR contributions appear near $\nu_k(^{17}O)$ upon growth has not yet been investigated completely. Further measurements are underway.

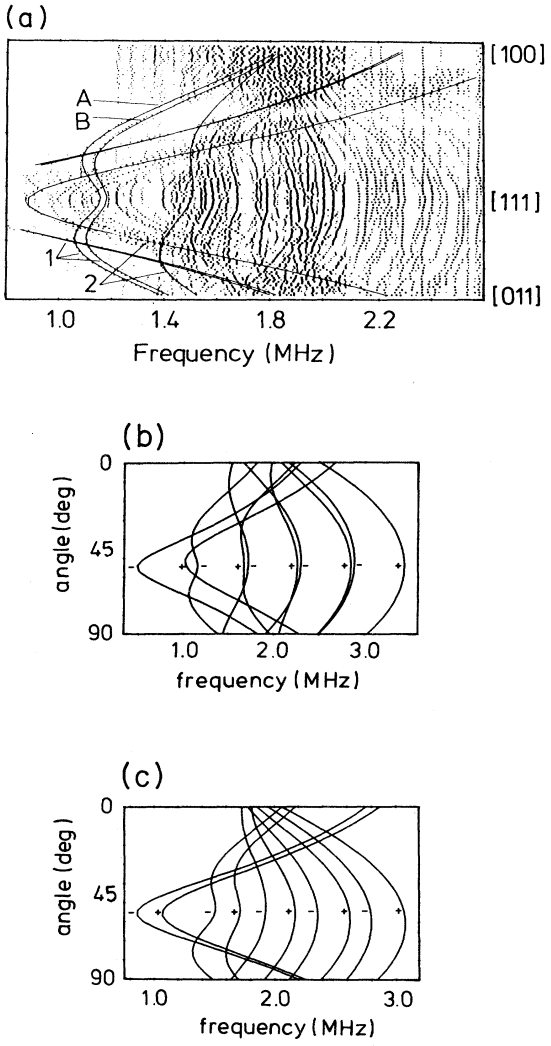

FIG. 16. Angular dependence of ^{17}O ENDOR lines of $(TD)^+$ centers in FZ-Si. The magnetic field $\mathbf{B}_0$ was rotated in a {110} plane. $\mathbf{B}_0$ was set to follow the ESR angular dependence of center orientations 2 and 3 [see Fig. 4(b)]. (a) Dots, experimental line positions; solid lines, some calculated angular dependencies with the shf- and quadrupole-interaction constants of Table I for $(TD)^+$ species *A* and *B*. (b) Calculated angular dependence for shell-1 oxygens and $(TD)^+$-center orientation 2. The + and − signs correspond to $m_s = +\frac{1}{2}$ and $-\frac{1}{2}$, respectively. (c) Calculated angular dependence for shell-2 oxygens and $(TD)^+$-center orientation 2. The + and − signs correspond to $m_s = +\frac{1}{2}$ and $-\frac{1}{2}$, respectively.

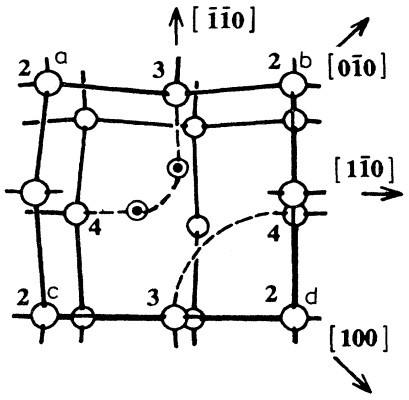

FIG. 17. View of the defect core along a [001] axis, if it contained only two oxygen atoms. 2–4 refer to the Si neighbor shells. The open circles represent Si; the open circles with a solid circle inside represent oxygen.

It would be tempting to conclude that the addition of further atoms upon TD growth must occur in pairs, since the C_{2v} symmetry was found to be preserved. We cannot, however, provide any physical mechanism for such an addition. If, of course, the addition of only one atom outside the core of the TD does not change the electronic structure enough as to split the ENDOR lines of the ^{29}Si and ^{17}O nuclei near or in the core, then also addition of a single atom can occur. Recent ENDOR observations on the NL10 defect in Al-doped Si, however, showed that upon growth the NL10 structure changes from C_{2v} to monoclinic symmetry, and it was concluded that single O atoms are added during growth. The suggested basic structure of NL10 contains two oxygens in a {110} plane.[5]

From our ENDOR results it is also clear that the TD core does not contain any acceptors—neither B nor Al was found. This is in agreement with recent ir investigations of the formation kinetics in undoped, B-doped, and Al-doped Cz-Si. It was found that the TD formation kinetics are identical for undoped and B-doped material.[26,27] In the presence of Al the NL8 formation is slower; mainly NL10 defects are formed, which indeed contain Al as part of their structure.[5] Al influences the oxygen precipitation so that new and different defects, mainly NL10,[18] are formed.

Without a wave function for the $(TD)^+$ it is not possible to derive the sites of the measured nuclei from the measured shf interactions. Here, the analysis of ENDOR spectra has its limitations. Our assignment of the observed ^{17}O to the TD core and the identified Si shells to the nearby Si ligands assumes that the wave function will fall off with distance monotonously. If this is not true, then another assignment compatible with the symmetry

properties of the defect is possible. Figure 18 shows what can be concluded from the ENDOR analysis: there are two oxygens on each {110} mirror plane with their shf and quadrupole tensors oriented approximately along ⟨111⟩ orientations. Whether the four oxygen atoms occupy a Si vacancy or whether another configuration compatible with the {110} mirror-plane symmetry and tensor orientations is realized, we cannot say from the ENDOR analysis. The position of the single-type-1-shell Si is not known along the [001] axis. Its position indicated in Fig. 10 is only an assumption. The center of the defect deviates somewhat from tetrahedral symmetry (see Table I). All model suggestions placing the oxygen atoms and possibly one interstitial Si in particular sites are speculation as long as their shf and quadrupole interactions are not explained by theory. Nevertheless, ENDOR has yielded the very important information that four oxygen atoms are involved in the core structure with a certain symmetry requirement which greatly narrows down possible structures.

In order to accommodate four oxygen atoms in a Si vacancy, one would have to relax the four nearest Si neighbors by approximately 15% outwards, which seems possible. Oxygen atoms could be bonded to the four Si neighbors along ⟨111⟩ directions and form bonding and antibonding states between themselves along the ⟨111⟩ directions. The antibonding state would be filled with two electrons and could qualitatively explain the double-donor nature of the TD's. However, a recent molecular-cluster calculation of such a model showed that this configuration requires a very high energy and it is not stable compared to other configurations.[28] In view of this it seems appropriate to discuss the observation of Si shell-type 1 in more detail. It is quite possible that it is

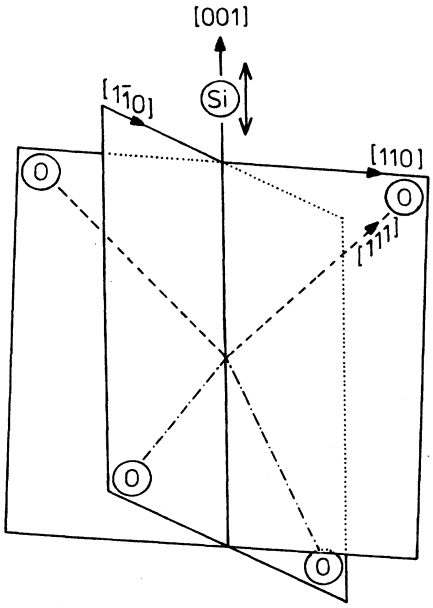

FIG. 18. $(TD)^+$ center core: Symmetry positions of the four oxygen atoms and shell-1 silicon as derived from ENDOR analysis.

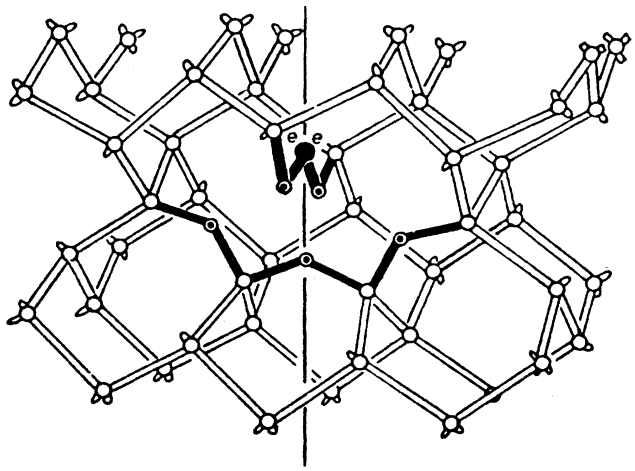

FIG. 19. OBS model for thermal donors, after Ref. 29. The *e*'s symbolize the donor electrons.

somewhere in the interstice along [001]. It cannot, however, be regarded as the "central-cell" part of an effective-mass-like donor because of its very low unpaired spin density (see below). It may have bonds with oxygen, which would lower the energy compared to the structure of four oxygens in a vacancy, but the resulting electron distribution must orient the shf-tensor *z* axis along [001].

The models currently discussed most are the Ourmazd-Bourret-Schröter (OBS) model[29] (Fig. 19) and the Y-Lid model[29,30] (see Fig. 20). In the OBS model one oxygen atom with [001] symmetry and two oxygen atoms on a (110) mirror plane would have been expected. We failed to see this single [001] oxygen atom. Instead, there are two oxygen atoms with different symmetries on the second (110) mirror plane. A cluster calculation for the OBS model predicted an anisotropic shf constant at the central ^{29}Si of about 80 MHz for the smallest $(TD)^+$.[32] The largest measured *b* value of a ^{29}Si is 2 orders of magnitude smaller. Therefore the OBS model core is incompatible with our ENDOR results. Similarly, in the Y-Lid model one single oxygen atom with [001] symmetry

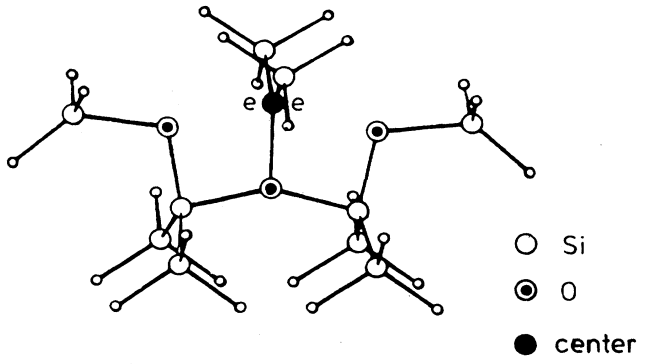

FIG. 20. Y-Lid model for thermal donors, after Refs. 30 and 31. The *e*'s symbolize the donor electrons.

would be expected with the most prominent oxygen interaction. Again, this is not observed. Also, the Y-Lid model is not compatible with the ENDOR results.

B. Electronic structure of the thermal donors

Perhaps the most striking feature of the shf interactions is the fact that they are all very small. Since the energy levels of the TD's are very shallow, one could expect to interpret the data with the effective-mass theory.[33] Indeed, comparison of the ^{29}Si interactions with those of the ^{29}Si ligands for the shallow donors P, As, and Sb in Si shows that they are very similar. For P in Si the largest values for the isotropic ^{29}Si shf constants are 6 MHz and those for the anisotropic shf constants are 0.4 MHz,[34] in good agreement with our findings. However, there the central nucleus has a much larger isotropic interaction (100–200 MHz), in contrast to what we find. If we assume that a central O atom would experience an isotropic interaction as predicted in the effective-mass theory, then we should have measured an isotropic constant $a(^{17}\mathrm{O})$ of approximately 50 MHz. The type-1-shell ^{29}Si cannot be a central atom either, according to effective-mass theory.[14]

The uniaxial-stress ESR and ir measurements[12,13] were explained assuming an approximate wave function for the TD, which is composed of a linear combination of only two conduction-band minima along [001]. In C_{2v} symmetry, there are combinations of conduction-band minima according to the A_1 (three times), A_2, B_1, and B_2 representations for an s electron. The A_2, B_1, and B_2 combination yields the result that the $\{100\}$ as well as the $\{110\}$ planes are nodal planes for the spin density, which is in contrast to our observations. Therefore, only the A_1 representations describe the $(\mathrm{TD})^+$ ground state. Any "central" nucleus would either have a large a (for symmetrical combinations) or large b (for antisymmetrical combinations) in the A_1 representation. There is no adequate theoretical model yet for a "cluster" within the effective-mass-theory framework. It is remarkable that the shf axes for the oxygens are along approximately $\langle 111 \rangle$, while all the Si neighbors have their axes along approximately [001]. The latter is a qualitative indication of a two-valley conduction-band minimum combination along [001], and for the fact that the wave function is very extended while the former points to the cluster nature in the core (also see Fig. 10). Such ligand axes were never found for deep defect centers.

If one estimates the localization of the unpaired electron on the observed nuclei simply with linear combination of atomic orbital expansion, one can account only for a few percent (approximately 5%) of the unpaired spin density. As seen also qualitatively in the very large "distant" ENDOR line in Fig. 5(a), most of the unpaired electron is strongly delocalized. Therefore, any cluster calculation, which may be undertaken presently, will not be able to calculate adequately the observed shf interactions simply because of the limited size of the cluster, which could be handled, but would have to contain a full unpaired electron. Here is certainly a challenge for theory.

VI. CONCLUSIONS

The ENDOR experiments have shown that the TD's contain oxygen atoms as an integral part of their structure. Four oxygen atoms with prominent shf interactions reside on the two (110) mirror planes of the $(\mathrm{TD})^+$ centers, which have C_{2v} symmetry within experimental accuracy. It is conceivable that one Si atom plays a particular role in connection with the four oxygen atoms to form the TD core. Further experiments are needed to decide whether the different $(\mathrm{TD})^+$ species identified both by ENDOR and ir are distinguished from each other by additional oxygen atoms or by additional Si atoms. The smallest TD seen in ENDOR is tentatively assigned to the third species seen in ir. From this species onwards all TD's have the same core.

[1] C. S. Fuller, J. A. Ditzenberger, N. B. Hannay, and E. Buehler, Phys. Rev. **96**, 833 (1954).

[2] C. S. Fuller and R. A. Lojan, J. Appl. Phys. **28**, 1427 (1957).

[3] W. Kaiser, H. L. Frisch, and H. Reiss, Phys. Rev. B **38**, 1546 (1958).

[4] H. H. P. Th. Bekmann, T. Gregorkiewicz, and C. A. J. Ammerlaan, Phys. Rev. Lett. **61**, 227 (1988).

[5] T. Gregorkiewicz, H. H. P. Th. Bekmann, and C. A. J. Ammerlaan, Phys. Rev. **38**, 3998 (1988).

[6] R. C. Newman, J. Phys. C **18**, L967 (1985).

[7] D. Mathiot, in *Defects in Electronic Materials,* edited by M. Stavola, S. J. Pearton, and G. Davies (MRS, Pittsburgh, 1988), Vol. 104, p. 189.

[8] P. Wagner, C. Holm, E. Sirtl, R. Öder, and W. Zulehner, in *Festkörperprobleme: Advances in Solid State Physics,* edited by P. Grosse (Vieweg, Braunschweig, 1984), Vol. 24, p. 191.

[9] P. Pajot, H. Compain, J. Lerouille, and B. Clerjaud, Physica B+C **117&118B**, 119 (1983).

[10] H. S. Muller, M. Sprenger, E. G. Sieverts, and C. A. J. Ammerlaan, Solid State Comm. **25**, 987 (1978).

[11] T. Gregorkiewicz, D. A. van Wezep, H. H. P. Th. Bekman, and C. A. J. Ammerlaan, Phys. Rev. B **35**, 3810 (1987).

[12] K. M. Lee, J. M. Trombetta, and G. D. Watkins, in *Microscopic Identification of Electronic Defects in Semiconductors,* edited by N. M. Johnson, S. G. Bishop, and G. D. Watkins (MRS, Pittsburgh, 1985), Vol. 46, p. 263.

[13] M. Stavola, K. M. Lee, J. C. Nabity, P. E. Freland, and L. C. Kimerling, in *Microscopic Identification of Electronic Defects in Semiconductors,* edited by N. M. Johnson, S. G. Bishop, and G. D. Watkins (MRS, Pittsburgh, 1985), Vol. 46, p. 257.

[14] J. Michel, J. R. Niklas, J.-M. Spaeth, and C. Weinert, Phys. Rev. Lett. **57**, 611 (1986).

[15] J. Michel, J. R. Niklas, and J.-M. Spaeth, in *Defects in Electronic Materials,* edited by M. Stavola, S. J. Pearton, and G. Davies (MRS, Pittsburgh, 1988), Vol. 104, p. 185.

[16] J. Michel, N. Meilwes, J. R. Niklas, and J.-M. Spaeth, in *Shallow Impurities in Semiconductors,* edited by B. Monemar (IOP, Bristol, 1988), Vol. 95, p. 201.

[17] T. Gregorkiewicz, D. A. van Wezep, H. H. P. Th. Bekman, and C. A. J. Ammerlaan, Phys. Rev. Lett. **59**, 1702 (1987).

[18]J. Michel, N. Meilwes, and J.-M. Spaeth, in *Defects in Semiconductors,* edited by G. Ferenczi (MRS, Budapest, 1988), Vols. 38–41, p. 607.
[19]H. Seidel, Z. Phys. **165**, 218 (1962); **165**, 239 (1962).
[20]J. R. Niklas, Habilitationsschrift, Universität Paderborn, 1983.
[21]M. U. A. Bromba and H. Ziegler, Anal. Chem. **55**, 648 (1983).
[22]J. R. Niklas, Radiat. Effects **72**, 39 (1983).
[23]P. Wagner (private communication).
[24]J. R. Niklas and J.-M. Spaeth, Phys. Status Solidi b **101**, 221 (1980).
[25]C. P. Slichter, *Principles of Magnetic Resonance with Examples from Solid State Physics* (Harper and Row, New York, 1963).
[26]I. Svensson, B. G. Svensson, and J. L. Lindström, Appl. Phys. Lett. **49**, 1435 (1986).
[27]M. Claybourn and R. C. Newman, in *Defects in Semiconductors,* edited by G. Ferenczi (MRS, Budapest, 1988), Vols. 38–41, p. 613.
[28]L. C. Snyder, P. Deck, R. Wu, and J. W. Corbett, in *Defects in Semiconductors,* edited by G. Ferenczi (MRS, Budapest, 1988), Vols. 38–41, p. 281.
[29]A. Ourmazd, W. Schröter, and A. Bourret, J. Appl. Phys. **56**, 1670 (1984).
[30]M. Stavola, and L. C. Snyder, in *Defects in Silicon,* edited by W. M. Bullis and L. C. Kimerling (Electrochemical Society, Pennington, NJ, 1983), p. 61.
[31]J. W. Corbett, J. C. Corelli, U. Desinca, and L. P. Snyder, in *Microscopic Identification of Electronic Defects in Semiconductors,* edited by N. M. Johnson, S. G. Bishop, and G. D. Watkins (MRS, Pittsburgh, 1985), Vol. 46, p. 243.
[32]J. Robertson and A. Ourmazd, Appl. Phys. Lett. **46**, 559 (1985).
[33]W. Kohn, in *Solid State Physics,* edited by F. Seitz and D. Turnbull (Academic, New York, 1957), Vol. 5.
[34]E. B. Hale and R. L. Mieher, Phys. Rev. **187**, 739 (1969).